

## Supporting materials for

# One-step *in situ* synthesis of BiOCl/(BiO)<sub>2</sub>CO<sub>3</sub> composite photocatalysts with exposed high-energy {001} facets

Yingying Chen, Yan Zhou, Qimei Dong, Hanming Ding

*School of Chemistry and Molecular Engineering, East China Normal University, 500*

*Dongchuan Road, Shanghai 200241, China*

### Contents:

- Fig. S1** The schematic diagram of crystal structure of BiOCl ( $2 \times 2 \times 2$ ) cells.
- Fig. S2** The schematic diagram of crystal structure of (BiO)<sub>2</sub>CO<sub>3</sub> ( $2 \times 2 \times 2$ ) cells.
- Fig. S3** XRD patterns of S(0.45) at different growth periods.
- Fig. S4** XRD pattern of (BiO)<sub>2</sub>CO<sub>3</sub>.
- Fig. S5** XRD patterns of the samples prepared under different pH values.
- Fig. S6** Nitrogen adsorption-desorption isotherms of various samples and the pore size distribution of S(0.45).
- Fig. S7** Kinetic fitting curves for photocatalytic decomposition of RhB over the different photocatalysts under visible light irradiation.
- Fig. S8** Time-dependent photocatalytic decomposition curves of RhB and phenol over S(0.45) under visible light irradiation.
- Fig. S9** The temporal changes of UV-vis spectra for RhB degradation over S(0.45) under UV light irradiation.
- Fig. S10** The Zeta-potential result of (BiO)<sub>2</sub>CO<sub>3</sub>, BiOCl(W), and S(0.45).
- Fig. S11** Comparison of the degradation efficiency of the prepared samples in our work for methyl orange (MO) degradation under visible light with that of the photocatalysts reported in literature.

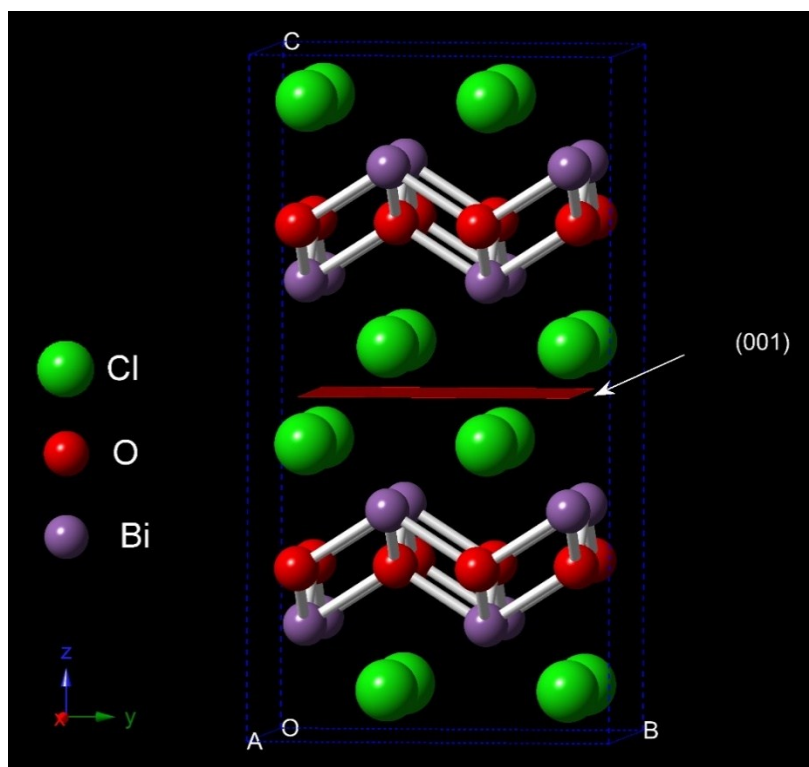


**Fig. S1** The schematic diagram of crystal structure of  $\text{BiOCl}$  ( $2 \times 2 \times 2$ ) cells.

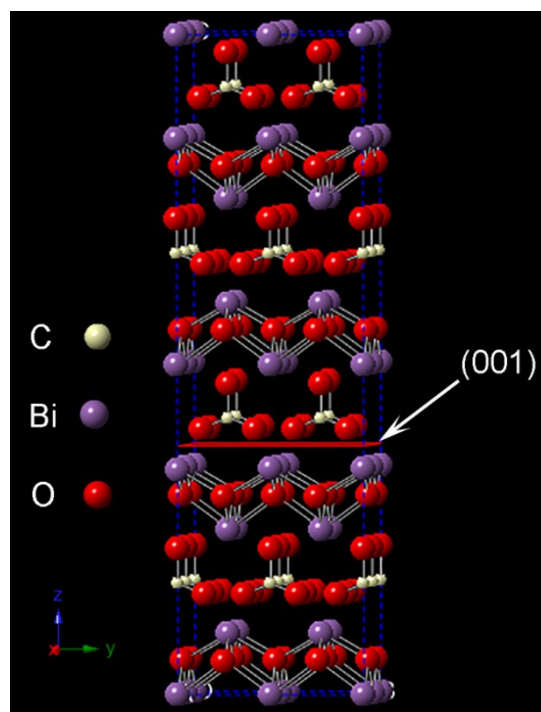


**Fig. S2** The schematic diagram of crystal structure of  $(\text{BiO})_2\text{CO}_3$  ( $2 \times 2 \times 2$ ) cells.

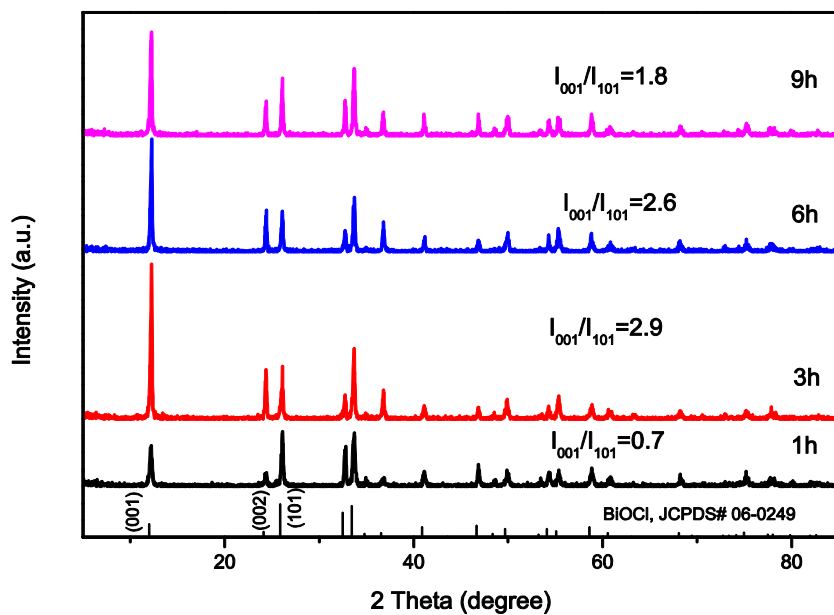


Fig. S3 XRD patterns of S(0.45) at different growth periods.

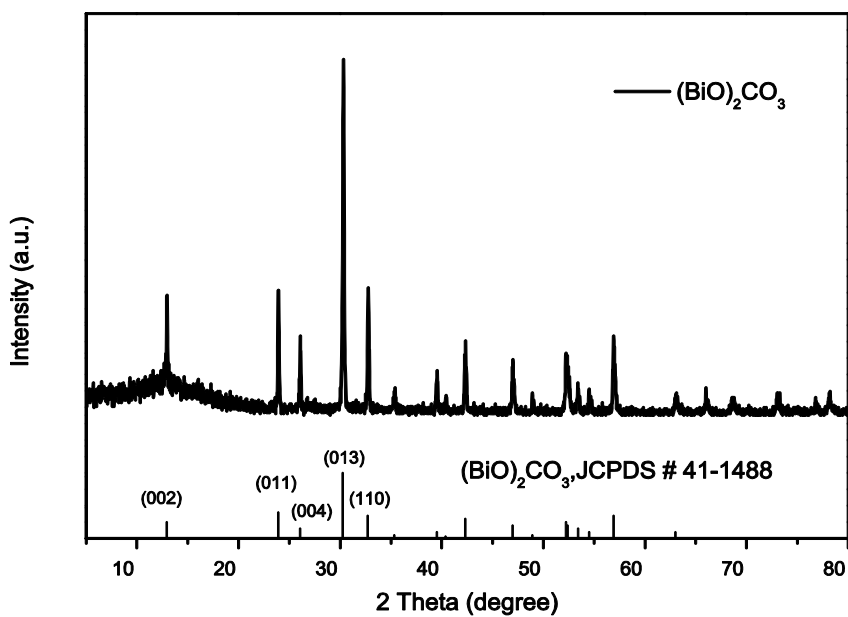


Fig. S4 XRD pattern of  $(\text{BiO})_2\text{CO}_3$ .

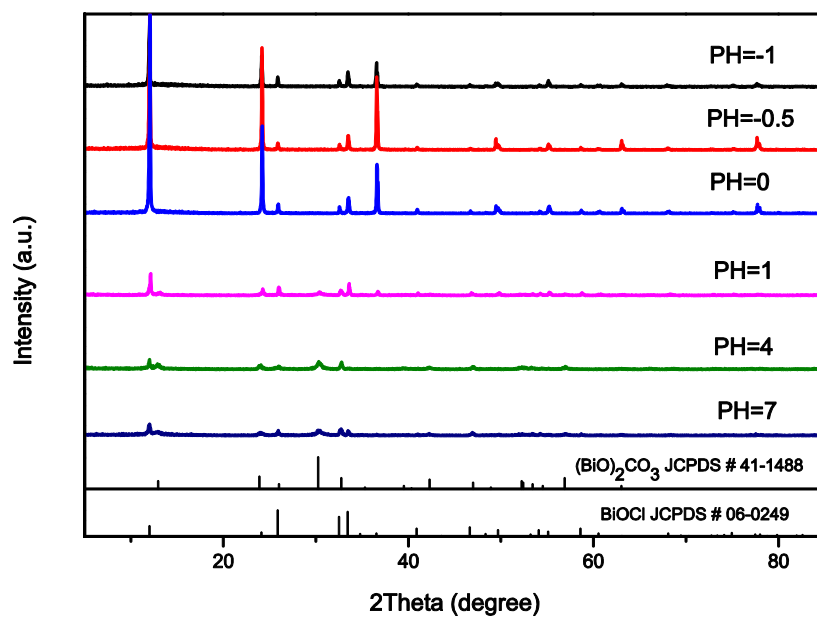


Fig. S5 XRD patterns of the samples prepared under different pH values.

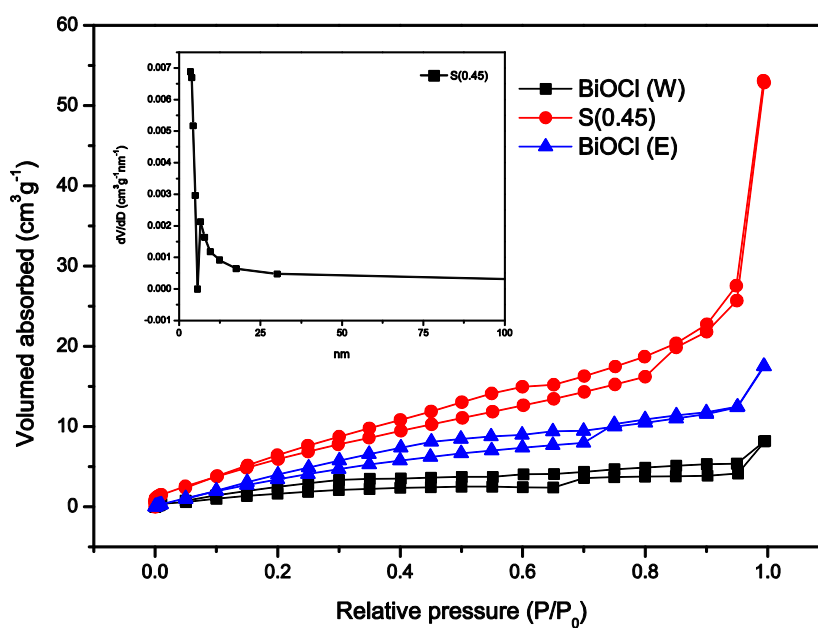
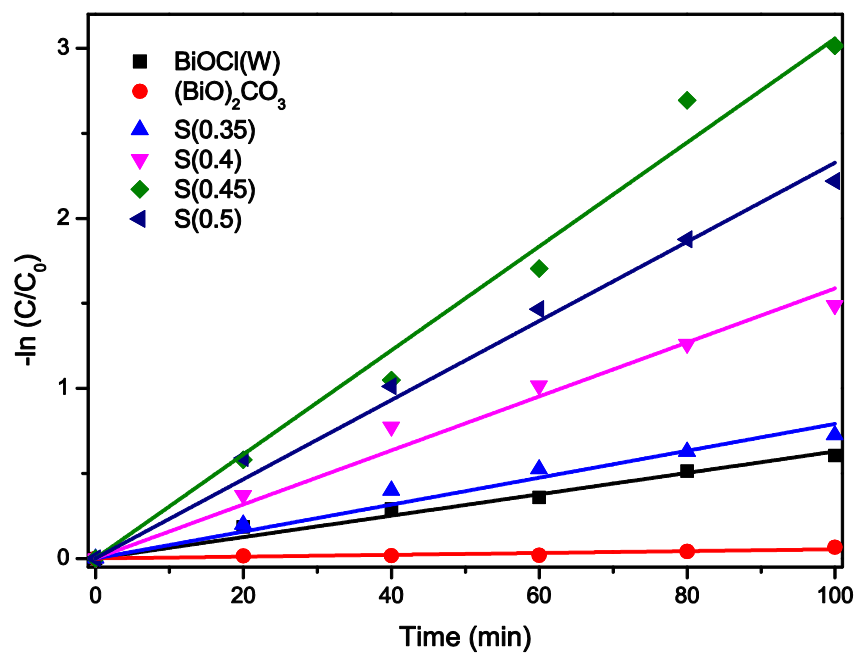
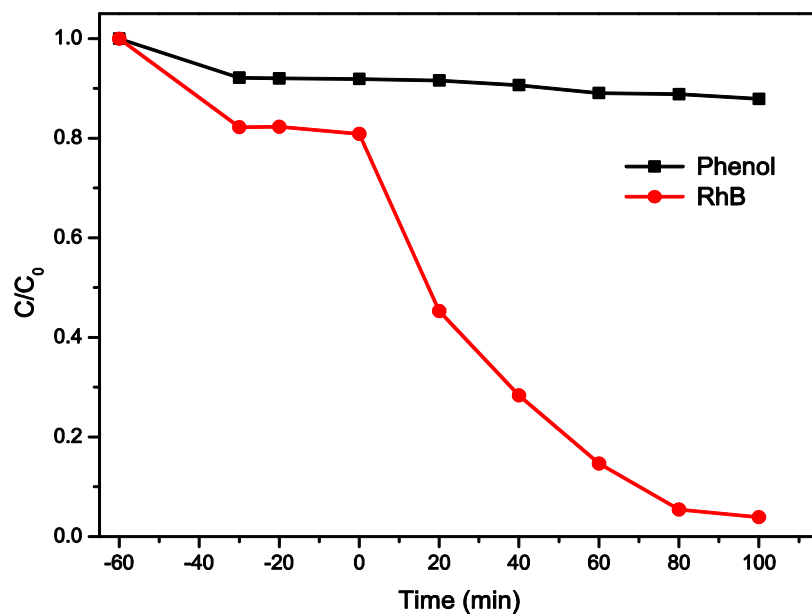


Fig. S6 Nitrogen adsorption-desorption isotherms of various samples. Inset: the pore size distribution of S(0.45).



**Fig. S7** Kinetic fitting curves for photocatalytic decomposition of RhB over the different photocatalysts under visible light irradiation.



**Fig. S8** Photocatalytic activity of S(0.45) for RhB and phenol degradation under visible light irradiation.

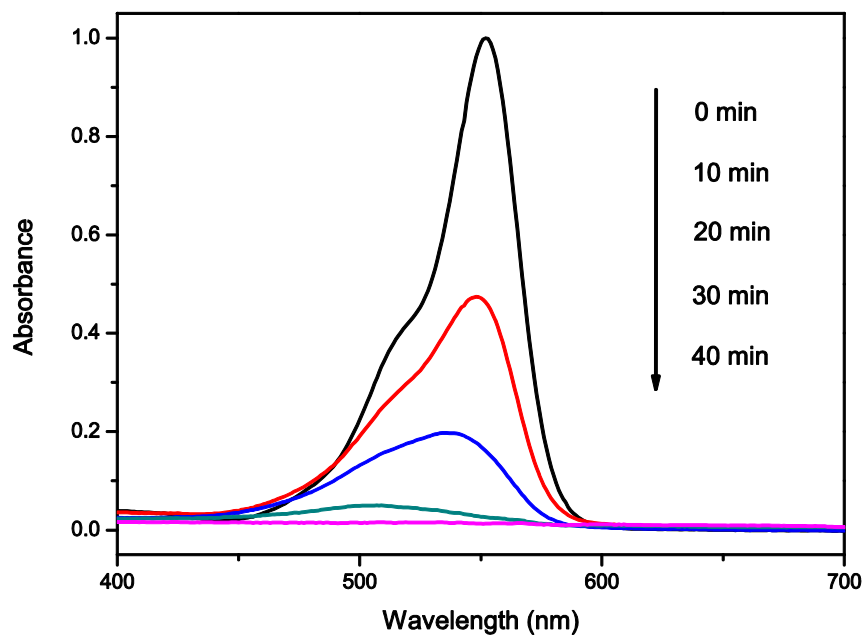


**Fig. S9** The temporal changes of UV-vis spectra for RhB degradation over S(0.45) under UV light irradiation.

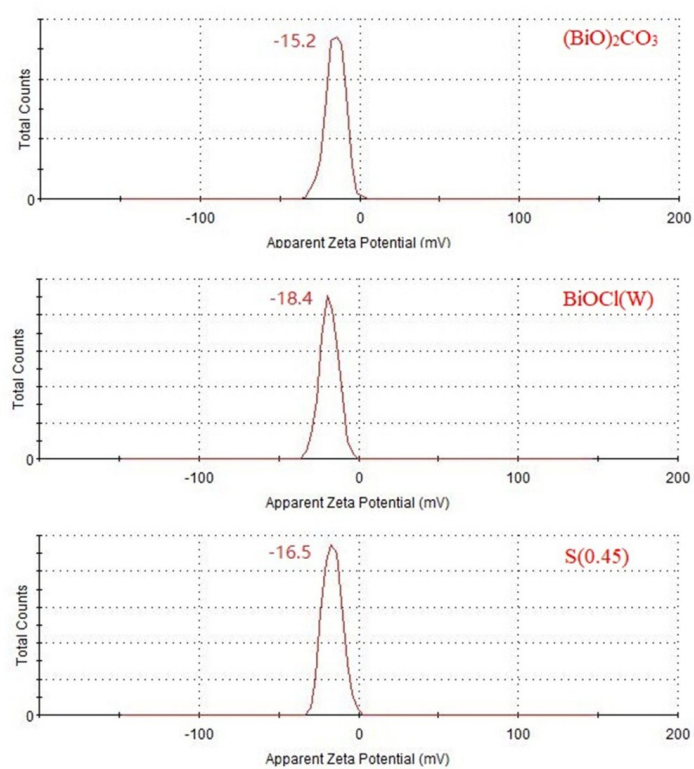


**Fig. S10** The Zeta-potential result of  $(\text{BiO})_2\text{CO}_3$ ,  $\text{BiOCl(W)}$ , and S(0.45).

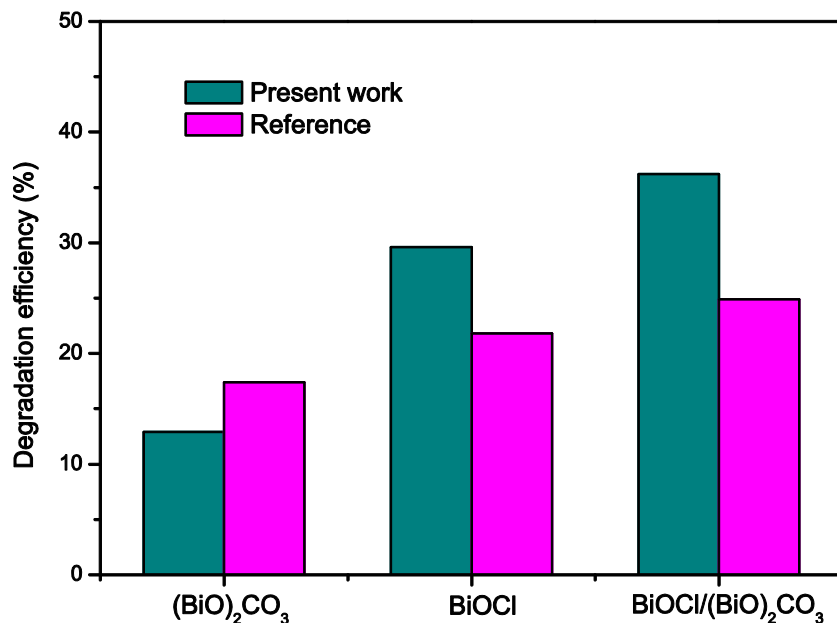


**Fig. S11** Comparison of the degradation efficiency of the prepared samples in our work for methyl orange (MO) degradation under visible light with that of the photocatalysts reported in literature.<sup>1</sup> Conditions: a photocatalyst (0.1 g) was suspended in 50 mL MO solution (10 mg·L<sup>-1</sup>). A 500 W Xe lamp with a 420 nm cutoff filter was employed as the visible-light source.

**Reference:**

1. J. Cao, X. Li, H. Lin, B. Xu, S. Chen and Q. Guan, *Appl. Surf. Sci.*, 2013, **266**, 294-299.